



HAL
open science

Coarse-Grained Model-Assisted Design of Polymer Prodrug Nanoparticles with Enhanced Cytotoxicity: A Combined Theoretical and Experimental Study

Ping Gao, Tâp Ha-Duong, Julien Nicolas

► **To cite this version:**

Ping Gao, Tâp Ha-Duong, Julien Nicolas. Coarse-Grained Model-Assisted Design of Polymer Prodrug Nanoparticles with Enhanced Cytotoxicity: A Combined Theoretical and Experimental Study. *Angewandte Chemie*, 2024, 10.1002/ange.202316056 . hal-04468750

HAL Id: hal-04468750

<https://hal.science/hal-04468750>

Submitted on 20 Feb 2024

HAL is a multi-disciplinary open access archive for the deposit and dissemination of scientific research documents, whether they are published or not. The documents may come from teaching and research institutions in France or abroad, or from public or private research centers.

L'archive ouverte pluridisciplinaire **HAL**, est destinée au dépôt et à la diffusion de documents scientifiques de niveau recherche, publiés ou non, émanant des établissements d'enseignement et de recherche français ou étrangers, des laboratoires publics ou privés.

Coarse-Grained Model-Assisted Design of Polymer Prodrug Nanoparticles with Enhanced Cytotoxicity: A Combined Theoretical and Experimental Study

Ping Gao,^{†,‡} Tâp Ha-Duong,^{*,†} and Julien Nicolas^{*,‡}

[†] *Université Paris-Saclay, CNRS, BioCIS, Orsay, 91400, France*

[‡] *Université Paris-Saclay, CNRS, Institut Galien Paris-Saclay, Orsay, 91400, France*

E-mail: tap.ha-duong@universite-paris-saclay.fr; julien.nicolas@universite-paris-saclay.fr

Abstract

To achieve drug release from polymer prodrug nanoparticles, the drug-polymer linker must be accessible for cleavage to release the drug, which can occur under certain physiological conditions (e.g., presence of specific enzymes). Supramolecular organization of polymer prodrug nanoparticles is crucial as it greatly affects the location of the linker, its surface exposure/solvation and thus its cleavage to release the drug. Since experimental access to these data is not straightforward, new methodologies are critically needed to access this information and to accelerate the development of more effective polymer prodrug nanoparticles, and replace the time-consuming and resource-intensive traditional trial-and-error strategy. In this context, we reported here the use of a coarse-grained model to assist the design of polymer prodrug nanoparticles with enhanced cytotoxicity. By choosing the solvent accessible surface area as the critical parameter for predicting drug release and hence cytotoxicity of polymer prodrug nanoparticles, we developed an optimized polymer-drug linker with enhanced hydrophilicity and solvation. Our hypothesis was then experimentally validated by the synthesis of the corresponding polymer prodrugs based on two different drugs (gemcitabine and paclitaxel), which demonstrated greater performances in terms of drug release and cytotoxicity on two cancer cell lines. Interestingly, our methodology can be easily applied to other polymer prodrug structures, which would contribute to the development of more efficient drug delivery systems via *in silico* screening.

Introduction

Prodrugs are molecules which are metabolized by living organisms into pharmacologically active drugs. Prodrugs are precursors of drugs and are primarily used to improve the bioavailability of drugs with unfavorable pharmacokinetic properties.^[1-5] They can also be used to improve drug selectivity to their intended target, thus reducing their undesirable side effects.^[6-10] When this concept is applied to polymers (i.e., by coupling drugs to polymers),^[11] the resulting polymer prodrugs can also take benefit from the polymer properties. They can for instance self-assemble into nanoparticles to efficiently protect drugs from early degradation, prolong their systemic circulation time, and deliver their payloads in diseased tissues by enhanced permeation and retention effect and/or via specific cleavage of the polymer-drug linker.^[12-17] The linker plays an essential role in polymer prodrug systems as not only does it prevent the uncontrolled “burst” release of the drug often experienced with non-covalent drug-loaded polymer nanocarriers, but it also controls the drug release kinetics and therefore the rate of prodrug metabolization into active drug, and ultimately therapeutic effect. To control the drug release from polymer prodrug nanoparticles, the polymer-drug covalent bond must be cleaved under specific conditions. This can be achieved by using pH-sensitive linkers,^[18] such as imines,^[19] amides,^[20] or hydrazones,^[21] which would be hydrolyzed only in acidic environment of diseased tissues. Alternatively, over-expression of specific enzymes in pathological sites/tissues, such as esterases or cathepsins, is another endogenous stimulus which can be used to cleave specific functional groups, such as ester or amide bonds.^[22-26]

Polymer prodrug nanoparticles are essentially obtained by formulation of the presynthesized polymer prodrugs, for instance by nanoprecipitation (also called solvent displacement/exchange method^[27]). Depending on the physico-chemical properties of the polymer prodrugs (e.g., water solubility of the drug and the polymer, position of the drug on the polymer chain), they will adopt a certain spatial organization during nanoparticle formation, which will have a significant impact on the localization of the drugs and, consequently, the linkers. This information is crucial because linkers embedded in the core of nanoparticles will not be easily accessible to enzymes or even solvated for hydrolytic cleavage, unlike linkers exposed at (or near) the surface. Unfortunately, experimental access to this information cannot be achieved by using routine colloids characterization techniques (e.g., dynamic light scattering, (cryogenic) transmission electron microscopy, etc.). Furthermore, while standard surface characterization techniques require dry

samples, which destructure nanoparticle morphology with low glass transition temperature (T_g) polymers, small angle scattering techniques are cumbersome experiments and not always relevant for quantifying the surface composition of nanoparticles.

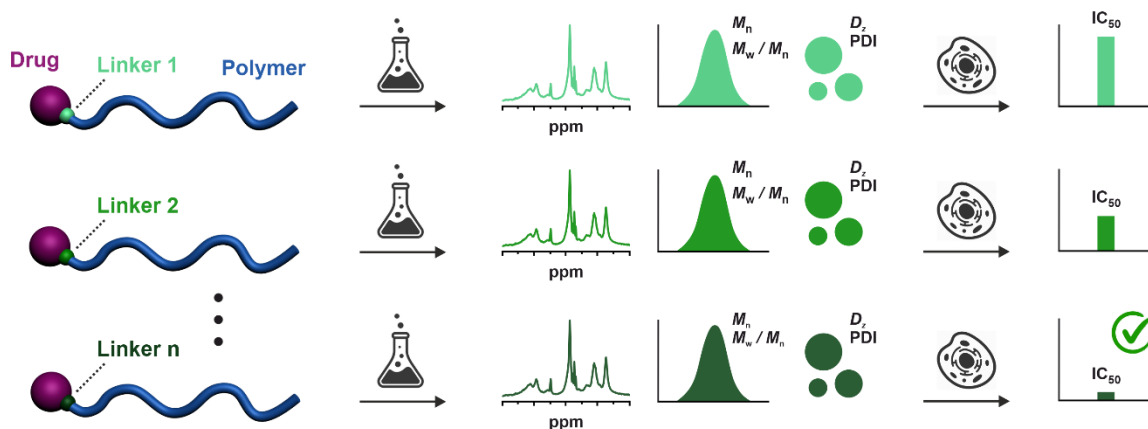
This is unfortunate because such precise and quantitative information would be valuable to effectively guide the development of new polymer prodrug nanoparticles. This explains, at least in part, why the evaluation of new drug delivery systems is almost exclusively based on the traditional trial-and-error strategy, which relies on synthesizing new structures and evaluating them *in vitro/in vivo*. However, this approach is time-consuming, costly and generates significant waste which is unsustainable. To circumvent these limitations, simulation of the supramolecular organization of polymer prodrugs may provide crucial atomic-scale information to predict and adapt the localization of key components (e.g., drugs, linkers) to accelerate the design of more potent drug delivery systems with minimal cost and resources.^[28]

Interestingly, coarse-grained modeling allows for simulations on longer time scales (2-3 orders of magnitude) and at a much lower computational cost than all-atom simulations, which is well suited for studies of supramolecular organization of macromolecules.^[29] Among the different models, MARTINI force fields, which were initially developed for lipid-based systems, can now be used for a broad range of supramolecular nanostructures,^[28, 30] including those based on polymers^[31-32] and short peptides.^[33-34] In this context, we have recently developed a MARTINI-based coarse-grained model to better understand the supramolecular organization of polymer prodrug nanoparticles based on gemcitabine-polyisoprene (Gem-PI) and paclitaxel-polyisoprene (Ptx-PI),^[35] which have previously shown promising results for anticancer therapy.^[36-37] In particular, we found that the nature of the polymer-drug linkage significantly influences its localization within the nanoassembly and thus its solvation, which could greatly influence the drug release and therefore the therapeutic effect.

However, whether this model can be used to predict, and even improve, the anticancer efficacy of polymer prodrug nanoparticles remains a critical question that could make this modeling approach of immense interest in drug delivery if it turns out to be the case. Herein, we applied our previously-developed coarse-grained model^[35] to the design of an optimized polymer-drug linker with enhanced hydrophilicity and solvation to: (i) avoid the tedious trial-and-error strategy and (ii) produce more effective polymer prodrug nanoparticles than those experimentally obtained so far (Figure 1). We demonstrated the reliability and the

versatility of this modeling approach by its experimental validation on polymer prodrugs based on two different drugs, in terms of drug release and cytotoxicity on two different cancer cell lines. While our previous study was more descriptive and of fundamental interest,^[35] the present work allows us to exploit the full potential of this coarse-grained approach by transforming it into an effective and sensitive predictive tool for the design of polymer prodrug nanoparticles with enhanced cytotoxicity.

Traditional approach: trial and error



This work: Coarse-grained-assisted design

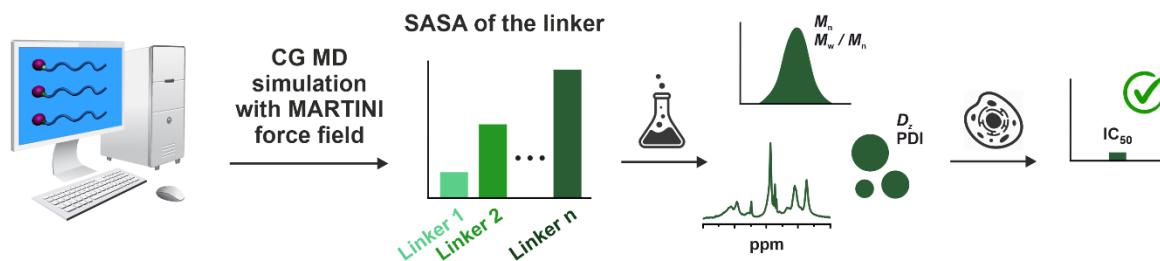


Figure 1. Schematic representation of the traditional trial-and-error approach and our coarse-grained (CG) molecular dynamic (MD) assisted design of polymer prodrug nanoparticles with enhanced cytotoxicity. M_n = number-average molar mass; M_w/M_n = weight-average molar mass / number-average molar mass (dispersity); D_z = intensity average diameter; PDI = polydispersity index; IC_{50} = half maximal inhibitory concentration; SASA = solvent accessible surface area.

Results and Discussions

General characteristics of polymer prodrug nanoparticles

The polymer prodrugs selected for improvement by coarse-grained model-assisted design were synthesized by the “*drug-initiated*” method (also termed “*grafting from*”),^[38] which relies on the controlled growth of a polymer chain from a drug molecule. This synthetic strategy has emerged as a robust yet simple approach as it requires only a few synthesis steps with high yields, and it permits easy adjustment of the polymer chain length and thus the drug loading. It is also very versatile as the nature of the drug, the linker and the polymer can be independently changed to gives access to a broad range of polymer prodrugs with tunable physicochemical and biological properties.

Among the different structures deriving from this synthetic strategy reported to date, Gem-PI and Ptx-PI polymer prodrugs (Figure 2a) were among the most promising ones owing to their surfactant-free formulation into nanoparticles exhibiting significant cytotoxicity against various cancer cell lines and anticancer efficacy in tumor-bearing mice.^[35-37] Two types of linkers were experimentally investigated at that time: an amide bond with Gem (Gem-*amide*-PI) and an ester-diglycolate sequence (*digly*) with Ptx (Ptx-*digly*-PI). Herein, to test our coarse-grained model-assisted design of polymer prodrugs in its ability to experimentally predict the influence of the nature of the linker on drug release and cytotoxicity, we simulated the supramolecular organization upon self-assembly of Gem- and Ptx-based prodrugs equipped with a novel, previously untested diglycolate-tetraethylene glycol (*digly*-TEG) linker (Figures 2a and 2b). This linker was designed to increase drug release and thus cytotoxicity through its greater hydrophilicity and surface exposure using the TEG moiety. Additional simulations and experimental investigations were also performed to establish linker structure-supramolecular organization-drug release-cytotoxicity relationships based on a total of three different linkers per drug type: (i) Gem-*digly*-PI, to investigate potential increase in cytotoxicity compared to Gem-*amide*-PI due to the greater lability of *digly* and (ii) Ptx-*propa*-PI, which is suspected to prevent efficient drug release because of its high hydrophobicity and steric hindrance (Figure 2a).

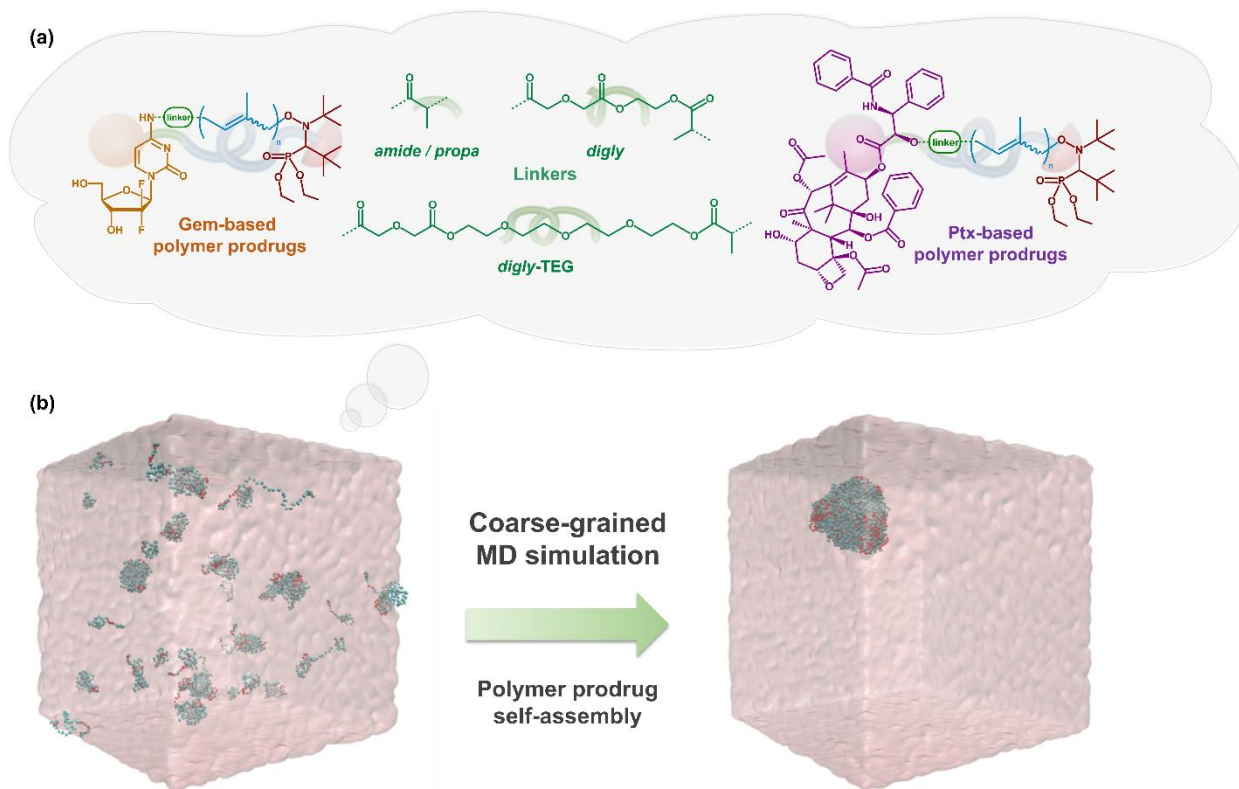


Figure 2. (a) Chemical structures of the different polymer prodrugs and linkers investigated in this study. Gem = gemcitabine; Ptx = paclitaxel; propa = propanoate; digly = diglycolate; TEG = tetra(ethylene glycol). (b) Coarse-grained molecular dynamics (MD) simulations of the polymer prodrug self-assembly.

Coarse-grained simulations of polymer prodrug nanoparticles

The self-assembly process of Gem-*digly*-TEG-PI and Ptx-*digly*-TEG-PI polymer prodrugs was monitored by calculating the number of aggregates and the number of chains in the largest one in their duplicate trajectories (Figure S4a). Simulations were carried out on the basis of 72 polymer chains, which represents a good compromise between reasonable computing time and obtaining a supramolecular organization less dependent on nanoparticle size.^[35] Results show that the randomly dispersed chains self-assemble into one aggregate in 11 μ s and 3 μ s for the Gem-based and Ptx-based polymer prodrugs, respectively. Furthermore, their self-assembly process is associated to a continuous decrease of the system free energy, indicating that the nanoparticle formation is a thermodynamics-driven spontaneous process (Figure S4b). The size of the aggregate was quantified by computing their radius of gyration (R_g) on parts of the trajectories where only one aggregate is observed (Figure S5). The longer the linker (*digly*-TEG > *digly* >

amide ~ propa), the higher R_g of the corresponding polymer prodrug aggregates for both drugs. In addition, the R_g values of Ptx-based aggregates were always higher than those of Gem-based aggregates regardless of the linker, probably due to the larger chemical structure of Ptx than Gem. These trends are nevertheless observed for a much lower number of chains than can be observed experimentally, where it is likely that the hydrophobicity of polymer prodrugs is the determining factor for nanoparticle size. It should also be noted that the modeled nanoparticles cannot be used to predict their pharmacodynamic properties, biodistribution, or drug accumulation, as only 72 chains were considered in our nanoparticle simulations to save computational time and resources, which is much smaller than in experimental nanoparticles.

Supramolecular organization of polymer prodrug nanoparticles

To study the supramolecular organization of the polymer prodrug nanoparticles, the trajectory parts of one self-assembled aggregate were analyzed. The radial distribution function (RDF) of the Gem-*digly*-TEG-PI and Ptx-*digly*-TEG-PI polymer prodrug components (i.e., Gem, Ptx, linker, PI and SG1), relative to the nanoparticle center of mass (COM) are displayed in Figure 3, and compared to those previously computed for polymer prodrug nanoparticles with *amide*, *propa* and *digly* linkers.^[35] It can be seen that PI mainly occupies the core of the *digly*-TEG-PI nanoparticles regardless of the nature of the drug, similarly to the other types of polymer prodrug nanoparticles. Interestingly, the density of PI in Gem-based nanoparticles is generally larger than in Ptx counterparts (the multiplying factors of PI RDF being larger in Gem- than Ptx-based nanoparticles). This can be explained by the fact that Ptx, being hydrophobic, is also occupying the core of the nanoparticles, partially pushing PI moieties outwards and reducing their density in the center, relatively to Gem nanoparticles. Conversely, whatever the type of linker, Gem was more distributed on the surface of the nanoparticles due to its hydrophilicity, whereas Ptx was more buried in the nanoparticle core due to its high hydrophobicity. Nevertheless, we calculated that 10–20% of Ptx molecular surface remains accessible to the solvent in the aggregates, making them partly visible on the surface of the nanoparticles (Figure 3). Since the surface area of isolated Ptx (10.3 nm²) is larger than that of Gem (4.6 nm²), the 10–20% of Ptx surface exposed to solvent still represents a larger area than that of their Gem-based counterparts, which explains why Ptx appears more visible than Gem on the nanoparticle surface in Figures 3a and 3b. Regarding the linkers, simulations of polymer prodrug nanoparticles based on the new *digly*-TEG linker established the trend whereby the spatial distribution of the linker is closer to the nanoparticle periphery as

its hydrophilicity increases: *propa/amide* < *digly* < *digly*-TEG. This trend is more pronounced for Gem-based polymer prodrug nanoparticles than in their Ptx-based counterparts, because the strongly hydrophobic Ptx can drag the linker deeper into the nanoparticle core than Gem can. The location of the potential cleavage sites (ester and amide groups) of the linkers was also investigated. The ester group from diglycolate next to the ethylene glycol moiety (*site 2*) is always located more closely to the surface of the nanoparticles compared to the amide/propa group near the drug (*site 1*) and the ester group near the PI chain (*site 3*), regardless of the nature of the drug. In addition, *site 2* moves closer to the surface of the nanoparticles as its hydrophilicity increased, while *site 1* and *site 3* showed only slight perturbation (Figure S6). Similarly to polymer prodrug nanoparticles based on the *amide*, *propa* and *digly* linkers,^[35] snapshots extracted from the simulation trajectories of polymer prodrug nanoparticles equipped with the new *digly*-TEG linker (Figure 3) revealed that drugs were inhomogeneously distributed on the surface of the nanoparticles. This was confirmed by the calculation of the drug pair correlation functions which exhibit a main peak at a distance equal to about twice the drug radius of gyration, indicating that the drugs are close to each other (Figure S7).

Changing the nature of the linker has a greater influence on its own location (especially the cleavage *site 2*) within the nanoparticles, rather than on the supramolecular organization of polymer prodrug nanoparticles and for instance on the location of the drugs.

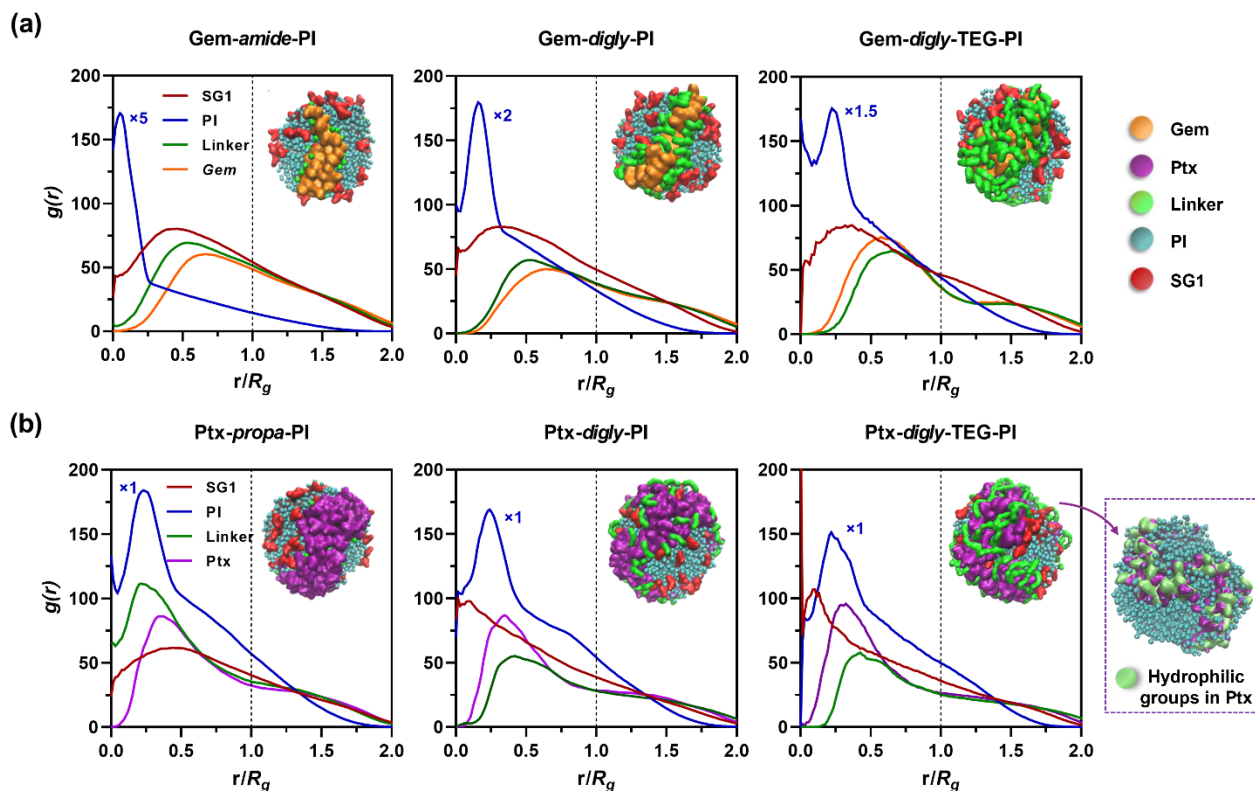


Figure 3. Radial distribution function ($g(r)$) of: (a) Gem-based and (b) Ptx-based polymer prodrug components relative to the center of mass of nanoparticles and their comparison between the polymer prodrugs with different linkers (the inner snapshots represent the corresponding nanoparticle supramolecular organization in coarse-grained model). For clarity purposes, the $g(r)$ of PI was scaled down and must be multiplied by the factor indicated in each graph to obtain the real values. r = radius, R_g = radius of gyration. Data on *amide*, *propa* and *digly* linkers are taken from ref ^[35].

Solvation and water-accessibility of the linkers

One of the critical factors in drug release from prodrug nanoparticles is the solvent-accessibility of the linkers (and in particular of the different cleavage sites, if any) which must be cleaved to release the drug. The Gem- and Ptx-based polymer prodrugs investigated in this work contain several cleavages sites (Figure 4a). Due to its higher hydrophilicity, the *digly*-TEG linker is distributed more on the surface of the nanoparticles than the *propa/amide* and *digly* linkers,^[35] which increases its water accessibility (Figures 3). Nevertheless, as illustrated from a snapshot of drug-*digly*-TEG-PI nanoparticles in water (Figure 4b), the three cleavage sites of the linker are not homogeneously solvated regardless the nature of drugs, which prompted us to further investigate their solvent-accessible surface area (SASA) values.

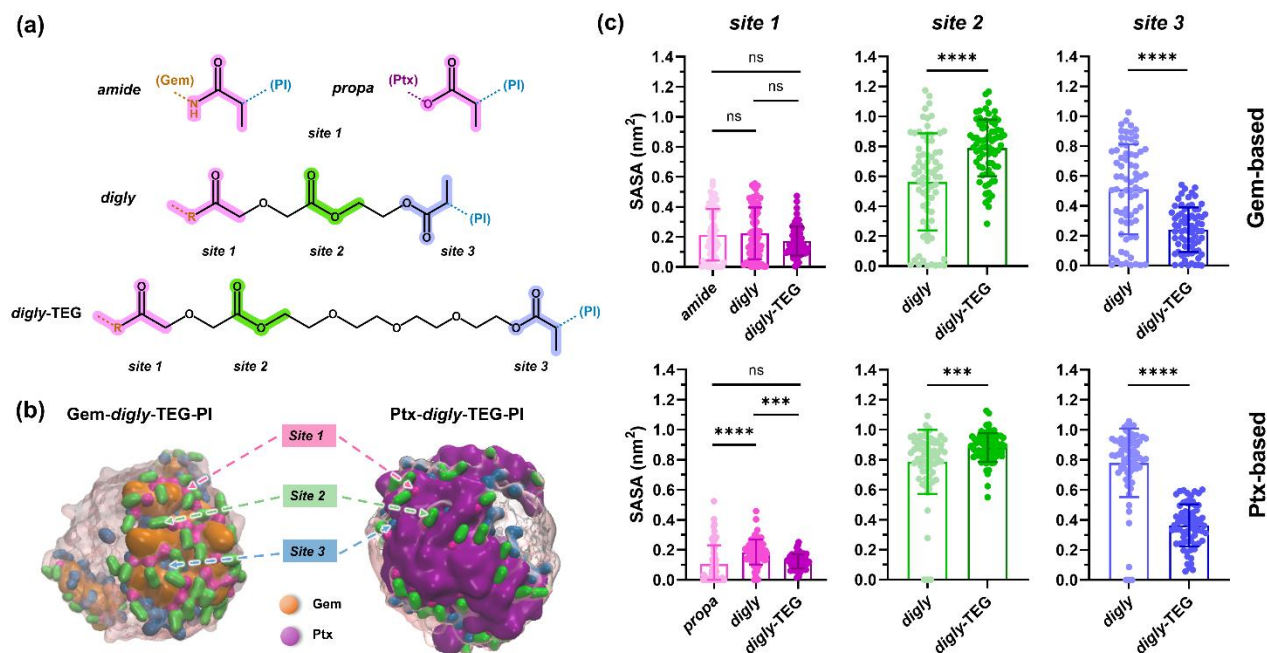


Figure 4. (a) Indication of the cleavage sites on the polymer prodrug chemical structures. (b) Location of the cleavage sites of the linkers shown on snapshots of Gem-*digly*-TEG-PI and Ptx-*digly*-TEG-PI nanoparticles in water (for the sake of clarity, PI and SG1 are made transparent). (c) Solvent-accessible surface area (SASA) of each cleavage site of *propa*, *amide*, *digly* and *digly*-TEG linkers, in Gem-based (top row) and Ptx-based (bottom row) polymer prodrug nanoparticles (the solid dots indicate the SASA distribution per residues in polymer prodrugs, $n = 72$). The values are expressed as the means \pm SD. For site 1: one-way ANOVA, with Tukey's correction for multiple comparisons; for sites 2 and 3: unpaired two-tailed t test; *** $p < 0.001$, **** $p < 0.0001$, ns = not significant. Data on *amide*, *propa* and *digly* linkers are taken from ref [35].

First, concerning the first cleavage site (*site 1*), an amide group sensitive to cathepsin B^[39] for Gem and an ester group sensitive to esterases^[40] for Ptx, it exhibits the lowest SASA values in both Gem-based and Ptx-based polymer prodrug nanoparticles (Figure 4c).^[35] Conversely, polymer prodrugs with linkers comprising multiple cleavage sites (i.e., *digly* and *digly*-TEG) present much higher SASA values. Interestingly, the SASA of the second cleavage site (*site 2*) of the *digly*-TEG linker is statistically significantly higher than that of the *digly* linker, both for Gem-based and Ptx-based polymer prodrug nanoparticles (Figure 4c). This difference in the SASA value of *site 2* is more pronounced in Gem-based nanoparticles than in Ptx-based ones, probably because the TEG moiety tends to pull *site 2* towards the nanoparticle surface but this effect is counterbalanced by the hydrophobicity of Ptx which tends to pull it towards the nanoparticle core. It can be noted that several *sites 2* of the *digly*-based polymer prodrug nanoparticles have SASA values close to zero (Figure 4c), reflecting the fact that they are completely

buried and inaccessible to the solvent, rather than being outliers. Interestingly, the number of these near-zero values is greater in *digly*-based polymer prodrug nanoparticles than in *digly*-TEG-based ones, probably because the hydrophobic PI chains pull the *sites 2* more inwards into the nanoparticle core in the former case than the latter.

The opposite tendency is observed for the third cleavage sites (*site 3*), probably because the *digly*-TEG linker is longer and more flexible than the *digly* one, allowing the propionyl moiety (*site 3*) to be more buried in the nanoparticle core. Note that *site 3* may result in poor drug release irrespectively of its location within the nanoparticles (Figure S6), because of its high steric hindrance.^[41] Taken together, our data suggest that *site 2* would be the preferred cleavage site and that polymer prodrugs based on the longer, more hydrophilic *digly*-TEG linker could lead, as hypothesized, to improved drug release and thus cytotoxicity than those based on *digly* or *propal/amide* linkers. Note that cleavage of *site 2* yields a drug-*digly*-related moiety whose release from the nanoparticle will facilitate cleavage of *site 1* and release of the parent drug.

The presence and spatial distribution of water molecules and counterions may have an impact on the hydrolytic and/or proteolytic cleavage of the drug-polymer linker. Therefore, we also analyzed the density of water molecules as well as sodium and chloride ions at the periphery of drug-*digly*-TEG-PI nanoparticles in our simulations (Figure 5). First, it appears that water molecules do not penetrate the nanoparticle core and remain on their surface, as their RDF values are equal to 0 below 0.4 nm and reached a first peak at ~0.5 nm. Near the nanoparticle surface, the RDF of sodium ions were systematically higher than those of chloride ions, which is consistent with the experimentally measured negative zeta-potentials. In addition, in line with their respective hydrophilic or hydrophobic nature, the density of ions (and water) at short distance from the drugs was higher for Gem than for Ptx. However, in both polymer prodrug nanoparticles, the cleavage *sites 2* remain strongly hydrated and surrounded by sodium counterions, to a significantly greater extent than in drug-*digly*-PI nanoparticles (Figure 5 vs Figure S13 from ref. ^[35]). These results indicate that cleavage of *site 2* by hydrolysis or enzymes would be easier in polymer prodrug nanoparticles equipped with the *digly*-TEG linker than those with the *digly* linker.

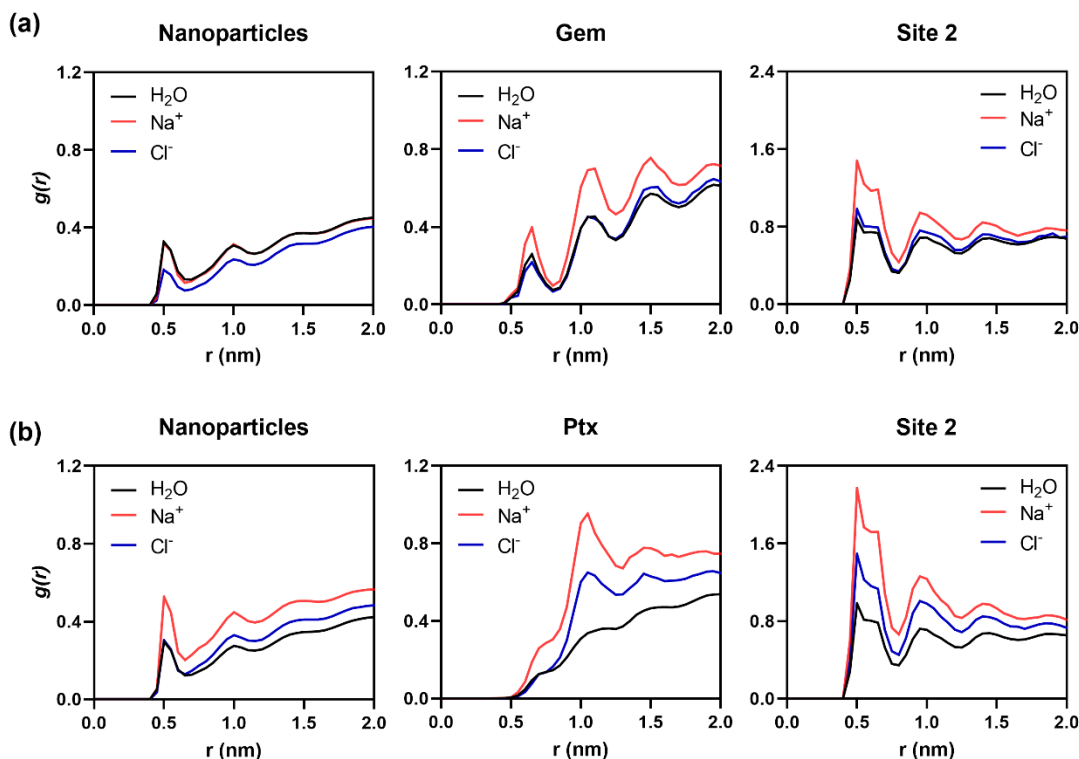


Figure 5. Radial distribution function ($g(r)$) of water (black), sodium (red), and chloride (blue) ions around: (a) Gem-*digly*-TEG-PI nanoparticles (left), Gem (middle), and cleavage site 2 (right) and (b) Ptx-*digly*-TEG-PI nanoparticles (left), Ptx (middle), and cleavage site 2 (right). r = radius.

Free energy calculation for the release of drug-*digly* moieties from the nanoparticles

Although cleavage of the linker is a key step, this parameter alone is not sufficient to fully describe drug release from polymer prodrug nanoparticles. To this end, we performed Umbrella Sampling simulations to account for drug interactions with the different nanoparticle components and solvent molecules. The free energy of the drug-*digly* (resulting from cleavage of *site 2*) unbinding process was computed to gain insight into the drug release kinetics of Gem and Ptx. As shown in Figure 6, the free energy cost for Ptx-*digly* release from the nanoparticle ($\Delta G = 17.0 \pm 0.01 \text{ kcal.mol}^{-1}$) is significantly higher than that of Gem-*digly* ($\Delta G = 6.8 \pm 0.01 \text{ kcal.mol}^{-1}$), indicating that efficiency of Ptx-*digly* release would be much lower than for Gem-*digly*.

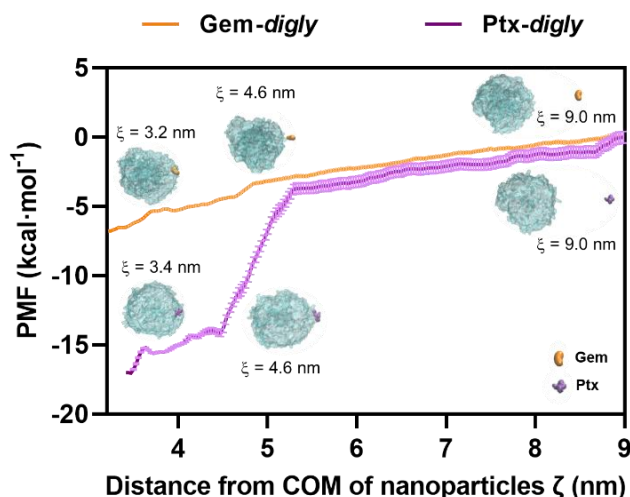


Figure 6. Free-energy profile, also called potential of mean force (PMF), of the release of Gem-*digly* (orange) and Ptx-*digly* (purple) from the corresponding polymer prodrug nanoparticles as a function of the distance from the center of mass (COM) of nanoparticles. The inner figures are snapshots of the drug release process at three different distances ($\xi = R_g$, 4.6 and 9.0 nm, respectively) in Gem-based and Ptx-based polymer prodrug nanoparticles. The transparent cyan material indicates the nanoparticles for better observation of the location of drug. The statistical errors were estimated from 100 bootstraps.

Experimental validation of the coarse-grained model-assisted design of polymer prodrugs

Synthesis of polymer prodrugs

To validate our coarse-grained model-assisted design of polymer prodrug nanoparticles with enhanced cytotoxicity, Gem-*digly*-TEG-PI and Ptx-*digly*-TEG-PI were synthesized for further evaluation. To experimentally evaluate the added value of the *digly*-TEG linker, Gem-*amide*-PI, Gem-*digly*-PI and Ptx-*digly*-PI were also synthesized for comparison. It should be noted that Ptx-*propa*-PI was not synthesized due to the lack of release from such a hindered ester linker bearing a methyl group in the α -position of the ester moiety, which is thought to prevent efficient solvation and enzyme access, as demonstrated with cladribine-*ester*-PI prodrug nanoparticles.^[41] Moreover, It has also been shown that Ptx-*ester*-squalene (squalene being a good model for PI)^[42] nanoparticles gave almost no cytotoxicity on cancer cells, despite a less sterically hindered ester linker, with IC₅₀ values in the tens of micromolar range.

All the polymer prodrugs were obtained by growing PI by nitroxide-mediated radical polymerization (NMP) from the corresponding drug-*linker*-functionalized alkoxyamine based on the SG1 nitroxide (Figure 7). More specifically, Gem (or Ptx) was linked under amidation (or esterification) reaction conditions to: (i) AMA-SG1, to yield Gem-*amide*-PI; (ii) *digly*-AMA-SG1, to yield Gem-*digly*-PI (or Ptx-*digly*-PI) and (iii) *digly*-TEG-AMA-SG1, to yield Gem-*digly*-TEG-PI (or Ptx-*digly*-TEG-PI). The different drug-functionalized alkoxyamines were successfully obtained and fully characterized by ^1H and ^{13}C NMR as well as mass spectrometry (see experimental part and Figures S2 and S3).

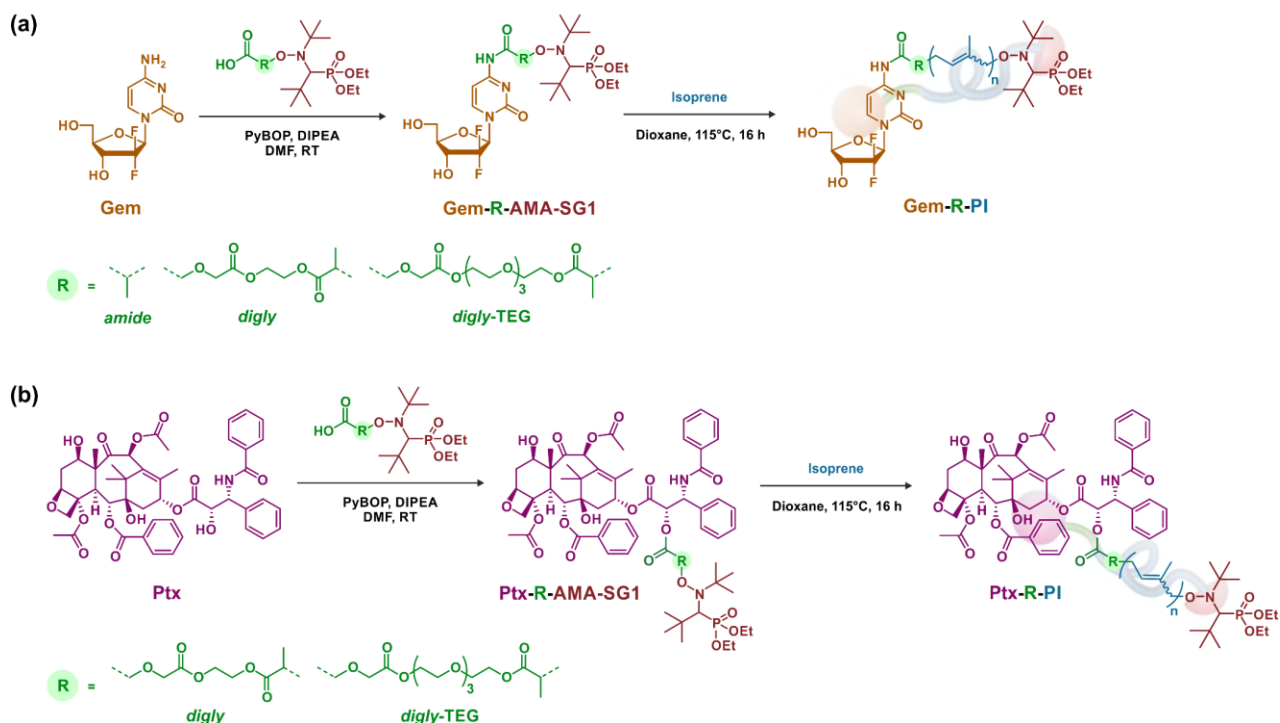


Figure 7. Chemical structures and synthesis strategies for: (a) Gem- and (b) Ptx-based alkoxyamine initiators and, their corresponding polymer prodrugs obtained by SG1-mediated nitroxide-mediated polymerization (NMP).

By using a [isoprene]₀:[alkoxyamine]₀ molar ratio of 200:1 to target small chain lengths and thus rather high drug loadings, well-defined Gem-based ($M_n \sim 2.5\text{--}3.0 \text{ kg}\cdot\text{mol}^{-1}$, $\mathcal{D} = 1.12\text{--}1.21$) and Ptx-based ($M_n \sim 3.0 \text{ kg}\cdot\text{mol}^{-1}$, $\mathcal{D} = 1.07\text{--}1.14$) polymer prodrugs were obtained (Table 1), as shown by SEC analyses (Figures 8a and 8b). The presence of the drugs at the extremity of the PI chains was confirmed by ^1H NMR spectroscopy based on the presence of proton signals characteristic of each drug; in particular the protons

from the aromatic pyrimidine rings of Gem ($\delta = 7.40-7.58$ and $7.90-8.12$ ppm) and the aromatic protons of Ptx ($\delta = 7.67-8.22$) (Figures 8c and 8d). These proton signals were also used to determine the M_n of the polymer prodrugs by comparing them to those of PI repeat units (Table 1), resulting in pretty good agreement between $M_{n,SEC}$ and $M_{n,NMR}$ values. The drug loading was about 9-11 wt % for Gem-based polymer prodrugs, and about 28-29 wt % for Ptx-based polymer prodrugs (Table 1). A drug free PI of similar M_n was also synthesized as a control by using the AMA-SG1 alkoxyamine under identical experimental conditions (Table 1). Note that there is no noticeable trend in M_n when increasing the size of the linker as: (i) the variation in linker length represents at most ~10 % of the total chain length (which is therefore difficult to detect by NMR and SEC which have measurement errors of this order of magnitude) and (ii) all PI chains are similar in length but not strictly identical.

Table 1. Macromolecular properties of Gem- and Ptx-based PI prodrugs, and colloidal properties of the corresponding nanoparticles.

Polymer prodrug	Conversion (%)	$M_{n,SEC}^a$ (g·mol ⁻¹)	\mathcal{D}^a	$M_{n,NMR}$ (g·mol ⁻¹)	D_z^e (nm)	PDI ^e	ζ (mV)	Drug loading ^g (wt %)
Gem- <i>amide</i> -PI	18	3010	1.21	3350 ^b	173	0.09	-30.0	8.8
Gem- <i>digly</i> -PI	14	2490	1.13	3680 ^b	168	0.01	-34.2	10.5
Gem- <i>digly</i> -TEG-PI	16	2500	1.12	3370 ^b	189	0.07	-44.2	10.5
Ptx- <i>digly</i> -PI	13	2980	1.11	3130 ^c	211	0.10	-36.1	28.7
Ptx- <i>digly</i> -TEG-PI	17	3040	1.07	3680 ^c	169	0.07	-32.8	28.1
PI	31	2320	1.14	1870 ^d	190	0.10	-40.0	–

^a Determined by SEC, calibrated with PS standards and converted into PI using Mark-Houwink-Sakurada parameters. It should be noted that these values must be taken with caution, as PI-based polymer prodrugs cannot be considered as PI homopolymers. ^b Calculated from ratio of areas under the peak at 7.40-7.58 and 7.90-8.12 ppm (aromatic pyrimidine H from Gem) and 5.0-5.5 ppm (vinylic H in isoprene repeat unit (1,4-addition), corresponding to 81.2% of total isoprene unit^[36]), according to $M_{n,NMR} = MW_{\text{alkoxyamine}} + DP_{n,NMR} \times MW_{\text{isoprene}}$. ^c Calculated from ratio of areas under the peak at 7.67-8.22 ppm (aromatic H from Ptx) over 5.0-5.5 ppm (vinylic H in isoprene repeat unit (1,4-addition), corresponding to 81.2% of total isoprene units), according to $M_{n,NMR} = MW_{\text{alkoxyamine}} + DP_{n,NMR} \times MW_{\text{isoprene}}$. ^d Calculated from ratio of areas under the peak at 3.1-3.3 ppm (α -H to P in SG1 moiety) over 5.0-5.5 ppm (vinylic H in isoprene repeat unit (1,4-addition), corresponding to 81.2% of total isoprene units), according to $M_{n,NMR} = MW_{\text{alkoxyamine}} + DP_{n,NMR} \times MW_{\text{isoprene}}$. ^e Determined by DLS. ^f Zeta potential. ^g %drug = $MW_{\text{drug}}/M_{n,SEC}$.

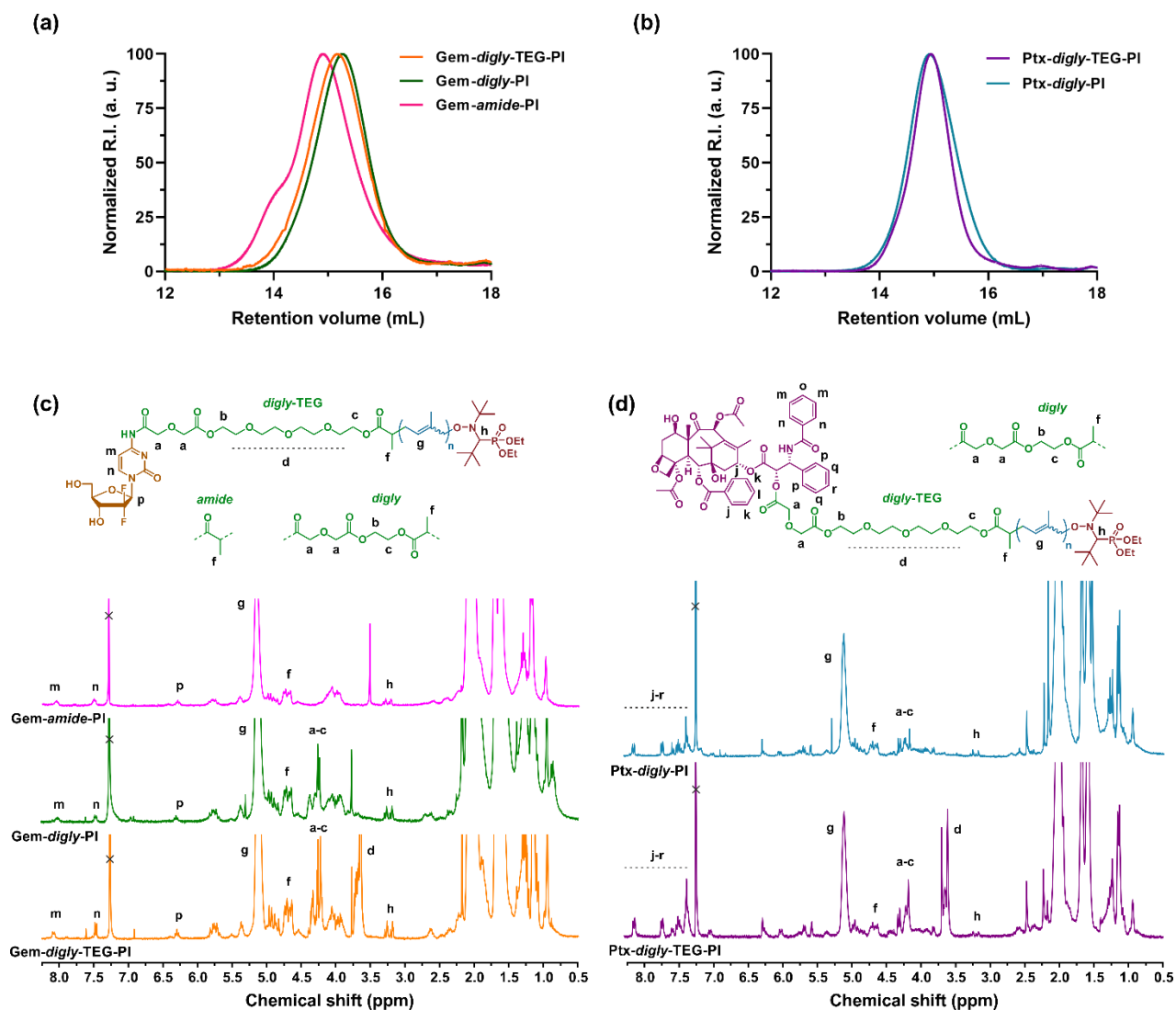


Figure 8. SEC chromatograms of: (a) Gem-based and (b) Ptx-based polymer prodrugs. ¹H NMR spectrum (300 MHz, CDCl₃) in the 0.5–8.5 ppm region of: (c) Gem-based and (d) Ptx-based polymer prodrugs.

Formulation of the polymer prodrug nanoparticles

Gem- and Ptx-based polymer prodrugs were then successfully formulated into surfactant-free nanoparticles by the nanoprecipitation technique^[27] at a final concentration of 1.0 mg·mL⁻¹. The polymer prodrug nanoparticles exhibited average diameters in the 168–218 nm range with low polydispersity values (0.01–0.10), as measured by DLS (Table 1). Such controlled average diameter within ~50 nm is important to rule out potential influence of the nanoparticle size on their biological evaluation (e.g., drug release, cell uptake).

The morphology of polymer prodrug nanoparticles was characterized by cryo-TEM (Figures 9a and 9b) or TEM (Figure S8), which demonstrated spherical shapes with average diameters and narrow particle size distributions, in rather good agreement with DLS measurements. Interestingly, the spherical shape obtained experimentally for both types of drug is consistent with that obtained by coarse-grained simulation. The colloidal stability of the polymer prodrug nanoparticles was assessed by DLS, which showed constant average diameters and dispersities in water for at least 40 days (Figures 9c and 9d). Overall, these results also show that the new *digly*-TEG linker has no detrimental influence on the nanoparticle formation and on their colloidal properties.

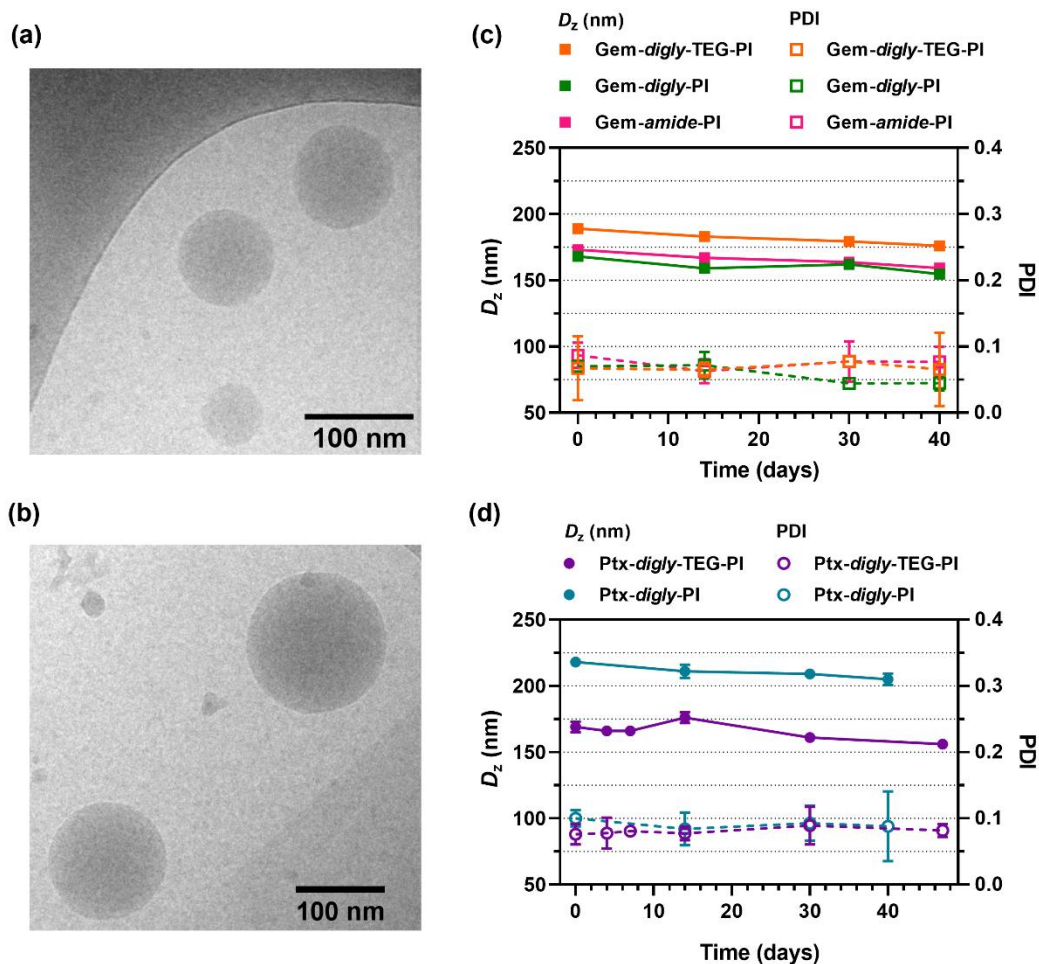


Figure 9. Representative Cryo-TEM images of: (a) Gem-*digly*-TEG-PI and (b) Ptx-*digly*-TEG-PI polymer prodrug nanoparticles. Evolution with time of the intensity-average diameter (D_z) and the polydispersity index (PDI) of: (c) Gem-based and (d) Ptx-based polymer prodrug nanoparticles. The values are expressed as the means \pm SD (n = 3).

Biological evaluations

Since coarse-grained simulations predicted higher solvent-accessible surface areas for the *digly*-TEG linker than for the *propal/amide* and *digly* linkers, Gem-*digly*-TEG-PI and Ptx-*digly*-TEG-PI polymer prodrug nanoparticles should lead to faster drug release (and thus greater cytotoxicity) than those made from the other linkers. To confirm this hypothesis, their drug release profile was monitored by HPLC at 37 °C in PBS and in human serum to mimic relevant biological environments. In PBS, Gem-*amide*-PI nanoparticles gave nearly no drug release (< 0.7 % after 48 h), whereas Gem-*digly*-PI and Gem-*digly*-TEG-PI nanoparticles exhibited ~4% and ~6% drug release, respectively, showing the beneficial effect of the *digly*-TEG linker (Figure 10a). The same effect was witnessed in human serum, in which Gem-*digly*-TEG-PI nanoparticles gave the highest drug release kinetics with ~19.5 % Gem released after 48 h, followed by Gem-*digly*-PI nanoparticles (~16 %) and Gem-*amide*-PI nanoparticles (1.1 %).

A similar trend was observed with Ptx-based polymer prodrug nanoparticles, as Ptx-*digly*-PI and Ptx-*digly*-TEG-PI nanoparticles gave very little Ptx release in PBS (~0.6 % after 48 h), whereas in human serum it reached 1.6 % and almost the double (3.0 %), respectively (Figure 10b). It should be noted that, according to the kinetic profile, a higher release of Ptx would certainly be achieved if the release was prolonged for a longer period. It should be noted that a maximum incubation time of 48 h was chosen for drug release kinetics, as both Gem and Ptx degrade in human serum over time.^[35, 43] This means that degradation kinetics are likely to be underestimated, while remaining comparable to each other.

These results first confirm the beneficial effect of adding a *digly* moiety compared with use of an amide bond alone because of its higher hydrophilicity and an additional labile group (ester) in its structure, which does not require the presence of specific enzymes to amide groups (e.g., cathepsins) as it is the case for Gem-*amide*-PI nanoparticles. More importantly, the results also confirm for both drugs the supplementary beneficial effect of adding a TEG moiety, which improves solvation of the linker and promotes surface exposition and drug release also in human serum.

Interestingly, for a given medium (PBS or human serum), drug release from Gem-based polymer prodrug nanoparticles was always higher than that from Ptx-based polymer prodrug nanoparticles, although the SASA values of their cleavable *site 2* are similar (Figure 4c). This observation is in agreement with the drug-nanoparticle and drug-solvent interactions previously determined by coarse-grained simulation (Figure 6). Indeed, as indicated by the PMF profile of the drug unbinding process, higher energy

is required to release Ptx-*digly* from nanoparticles in order to overcome the strong hydrophobic interactions between Ptx and the different nanoparticle components, compared to that required for Gem-*digly* (Figure 6).

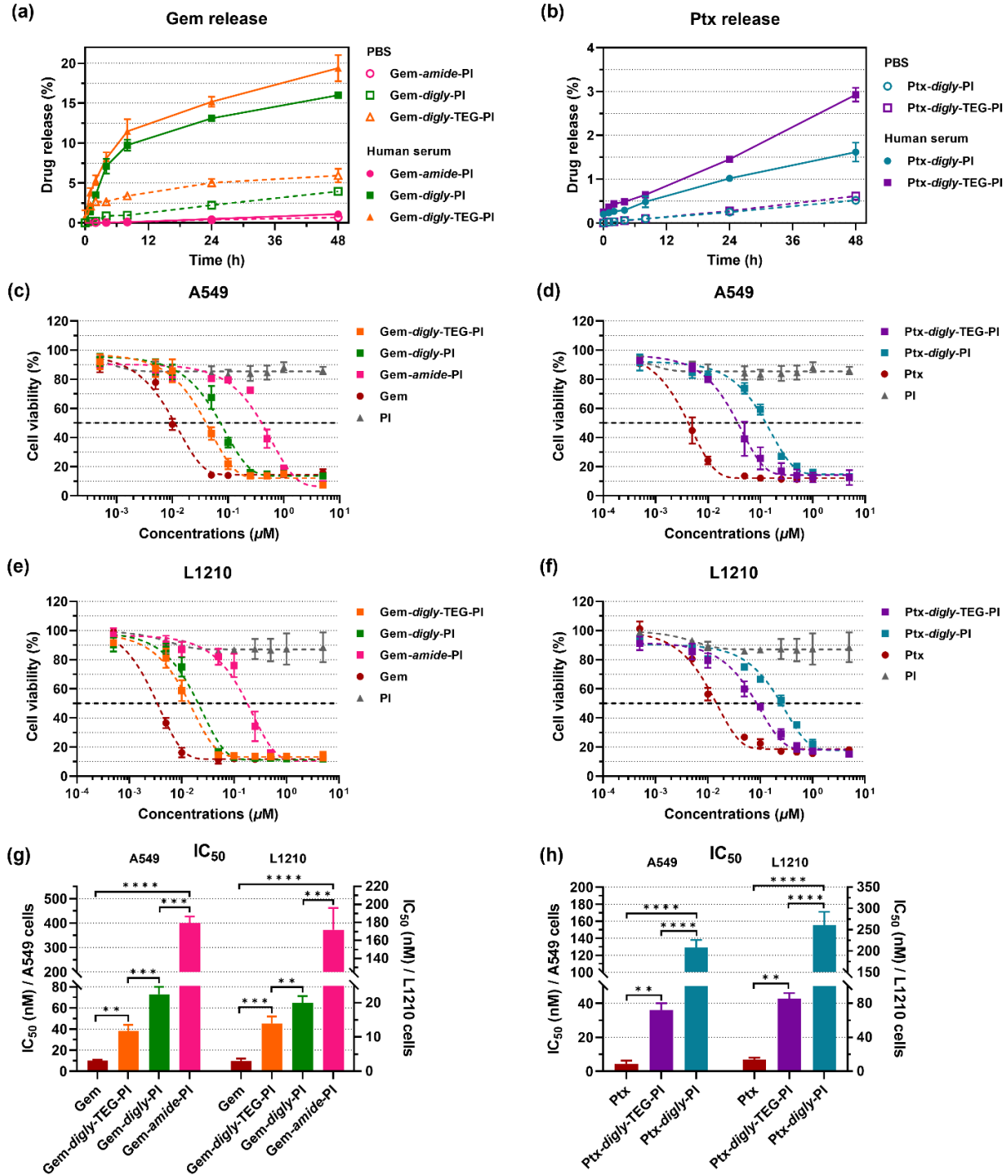


Figure 10. Drug release kinetics up to 48 h in PBS (open) or human serum (solid) at 37 °C obtained from: (a) Gem-*amide*-PI, Gem-*digly*-PI and Gem-*digly*-TEG-PI nanoparticles, and (b) Ptx-*digly*-PI and Ptx-*digly*-TEG-PI nanoparticles.

Evolution of the cell viability (MTT test) of (c and d) A549 cells and (e and f) L1210 cells after incubation with increasing concentrations of (c and e) Gem-*amide*-PI, Gem-*digly*-PI and Gem-*digly*-TEG-PI nanoparticles and (d and f) Ptx-*digly*-PI and Ptx-*digly*-TEG-PI nanoparticles, as well as (g, h) the corresponding IC₅₀ values. The values are expressed as the means ± SD. Unpaired two-tailed *t* test, ** *p* < 0.01, *** *p* < 0.001, **** *p* < 0.0001.

The *in vitro* cytotoxicity of the polymer prodrug nanoparticles was then evaluated by cell viability assay (MTT) on two relevant cancer cell lines: human lung cancer cells A549 and mouse leukemia cells L1210. Remarkably, as predicted by coarse-grained simulations, both Gem- and Ptx-based polymer prodrug nanoparticles showed increasing cytotoxicity with increasing linker hydrophilicity on both cell lines (Figures 10c–h). These results are also fully consistent with the release kinetics of Gem and Ptx (Figures 10a and 10b). Indeed, in both cell lines and for both drugs, polymer prodrug nanoparticles with the *digly*-TEG linker exhibited statistically lower IC₅₀ values than those with the *digly* and *amide* linkers (in that order). On A549 cells, IC₅₀ values of Gem-*amide*-PI, Gem-*digly*-PI and Gem-*digly*-TEG-PI nanoparticles were 400, 73 and 38 nM, respectively (Figures 10c and 10g), which is approaching the IC₅₀ of free Gem (10 nM). Similarly, Ptx-*digly*-PI and Ptx-*digly*-TEG-PI nanoparticles exhibited IC₅₀ values of 129 and 36 nM, respectively (Figures 10d and 10h), while IC₅₀ of free Ptx was 4 nM. The same trends were also observed on L1210 cells (Figures 9e–9h). Gem-*amide*-PI, Gem-*digly*-PI and Gem-*digly*-TEG-PI nanoparticles gave IC₅₀ values of 172, 20 and 14 nM, respectively, again approaching that of the parent drug (3 nM). For Ptx-*digly*-PI and Ptx-*digly*-TEG-PI nanoparticles, IC₅₀ values were 261 and 85 nM, respectively, with IC₅₀ of free Ptx equal to 14 nM. Overall, there is a fairly good relationship between relative differences in drug release kinetics and cytotoxicity, as the higher the difference in drug release, the higher the difference in IC₅₀. While the free drugs were more cytotoxic than any of the polymer prodrugs (as expected due the time needed for the drugs to be released), we also showed that the drug-free polymer (PI) was not cytotoxic at all concentrations tested in A549 and L1210 cells (Figures 10c–f), thus ruling out potential cytotoxicity of the polymer itself and confirming its cytocompatibility. Importantly, PI was obtained by polymerization of isoprene from the AMA-SG1 alkoxyamine initiator, which carries a carboxylic acid group to mimic the structure of the linkers after cleavage in order to assess their potential cytotoxicity once the drug had been released.

Interestingly, the beneficial effect of the TEG moiety on the drug release and cytotoxicity was more pronounced for Ptx-based prodrugs than for their Gem-based counterparts. This is probably due to the

hydrophilic nature of Gem which tends to attenuate the benefits of increasing the hydrophilicity of the hydrophilic linker on its solvation and cleavage, whereas they are greater for Ptx-based polymer prodrugs due to the strong hydrophobic nature of Ptx. In fact, this demonstrates the robustness and sensitivity of our coarse-grained model which can also predict small differences in cytotoxicity through accurate determination of the spatial distribution of linkers and calculation of their solvent accessible surface areas, which represents the determining factor.

Conclusion

In this work, we have developed and applied a molecular modeling approach based on MARTINI CG force fields, originally used to describe the supramolecular organization of polymer prodrug nanoparticles, to guide the development of drug-polymer linkers and accurately predict their relative cytotoxicity on cancer cells in order to discover optimized polymer prodrug structures. We relied on the calculation of SASA values of the different cleavage sites of the linkers developed so far (i.e., *propa*, *amide* and *digly*), and we successfully proposed a new linker, *digly*-TEG, with increased hydrophilicity and surface exposure according to our simulations. The hypothesis and prediction that increasing the SASA value of the linker would increase the drug release and the cytotoxicity were then experimentally validated by synthesizing the corresponding polymer prodrugs based on either Gem or Ptx, and by investigating their drug release kinetics in PBS or in human serum and their cytotoxicity on 2 different representative cancer cell lines. Importantly, the results showed that increasing the linker hydrophilicity (*propa/amide* < *digly* < *digly*-TEG) resulted in increased drug release and cytotoxicity, in perfect agreement with our simulations and hypothesis. This CG model-assisted design of polymer prodrug nanoparticles is robust and highly versatile as it has been validated on polymer prodrugs based on two different drugs, three different linkers and two cancer cell lines.

Importantly, due to the transferable building block philosophy of the MARTINI force fields, new linkers can be easily implemented in existing CG models as only their bonded parameters have to be defined. This

greatly simplifies the mapping and CG model building procedures, and allows for accelerating the determination of more promising structures.

To the best of our knowledge, this work represents the first example of using SASA values from a CG model to experimentally predict drug release kinetics and optimize the cytotoxicity of polymer prodrug nanoparticles. By made it possible to move from passive CG-assisted description of the supramolecular organization of polymer nanoparticles to active CG-assisted prediction of their cytotoxicity, this approach could make it possible to avoid numerous screening experiments in cell cultures, save a great deal of time, reduce costs and, above all, reduce, or even potentially eliminate, animal experimentation. This last point is extremely important in the context of the 3Rs principles (Replacement, Reduction and Refinement), the aim of which is to achieve more humane animal research.^[44]

There is still a long way to go before we can directly model drug delivery systems optimized for preclinical development, with superior *in vivo* performances. Particularly, the prediction of polymer prodrug nanoparticle absolute drug release kinetics *in vivo* remains extremely complex and challenging since many parameters and conditions can influence drug release *in vivo*, including pH and/or the concentration of specific enzymes in the disease tissues. However, this work provides solid evidence that CG simulation could be used as an accurate and prospective tool to better understand the supramolecular organization of various types of drug delivery systems and predict crucial physico-chemical properties and relative drug release efficiency, in order to more rapidly improve their therapeutic efficacy, which should be of great interest in the field of nanomedicine.

Acknowledgement

The authors thank Dr. Julie Mougín and Stéphanie Denis (Institut Galien Paris-Saclay) for technical assistance in (Cryo-)TEM and cell culture, respectively. The authors acknowledge the financial support from the China Scholarship Council (fellowship 20190835003). This work was supported by HPC resources from GENCI-IDRIS (grant A0070710968). The CNRS and University Paris-Saclay are also acknowledged for financial support.

Table of Content Graphic and Text



By choosing the solvent accessible surface area as the critical parameter for predicting relative drug release and hence cytotoxicity of polymer prodrug nanoparticles, we developed an optimized polymer-drug linker with enhanced hydrophilicity and solvation. Our hypothesis was experimentally validated by the synthesis of the corresponding polymer prodrugs based on two different drugs, which demonstrated greater drug release and cytotoxicity on two cancer cell lines.

References

- [1] M. Ninomiya, K. Tanaka, Y. Tsuchida, Y. Muto, M. Koketsu, K. Watanabe, *J. Med. Chem.* **2011**, *54*, 1529-1536.
- [2] S. Dhaneshwar, K. Tewari, S. Joshi, D. Godbole, P. Ghosh, *Chem. Phys. Lipids* **2011**, *164*, 307-313.
- [3] Y. Li, Y. Wang, R. Zhang, C. Liu, Y. Wei, J. Sun, Z. He, Y. Xu, T. Zhang, *Drug Deliv. Transl. Res.* **2018**, *8*, 1335-1344.
- [4] B. S. Vig, K. M. Huttunen, K. Laine, J. Rautio, *Adv. Drug Deliv. Rev* **2013**, *65*, 1370-1385.
- [5] C. E. Müller, *Chem. Biodivers.* **2009**, *6*, 2071-2083.
- [6] Y. Ikeda, H. Hisano, Y. Nishikawa, Y. Nagasaki, *Mol. Pharm.* **2016**, *13*, 2283-2289.
- [7] Y. Amitay, H. Shmeeda, Y. Patil, J. Gorin, D. Tzemach, L. Mak, P. Ohana, A. Gabizon, *Pharm. Res.* **2016**, *33*, 686-700.
- [8] J. Mayr, P. Heffeter, D. Groza, L. Galvez, G. Koellensperger, A. Roller, B. Alte, M. Haider, W. Berger, C. R. Kowol, B. K. Keppler, *Chem. Sci.* **2017**, *8*, 2241-2250.
- [9] H.-K. Han, G. L. Amidon, *AAPS PharmSci* **2000**, *2*, 48-58.
- [10] R. Mahato, W. Tai, K. Cheng, *Adv. Drug Deliv. Rev* **2011**, *63*, 659-670.
- [11] V. Delplace, P. Couvreur, J. Nicolas, *Polym. Chem.* **2014**, *5*, 1529-1544.
- [12] R. Duncan, *Nat. Rev. Drug Discov.* **2003**, *2*, 347-360.
- [13] X. Wei, Q. Luo, L. Sun, X. Li, H. Zhu, P. Guan, M. Wu, K. Luo, Q. Gong, *ACS Appl. Mater. Interfaces* **2016**, *8*, 11765-11778.
- [14] A. Bordat, T. Boissenot, N. Ibrahim, M. Ferrere, M. Levêque, L. Potiron, S. Denis, S. Garcia-Argote, O. Carvalho, J. Abadie, C. Cailleau, G. Pieters, N. Tsapis, J. Nicolas, *J. Am. Chem. Soc.* **2022**, *144*, 18844-18860.
- [15] A. Nguyen, R. Böttger, S.-D. Li, *Biomaterials* **2021**, *275*, 120955.
- [16] D. Trung Bui, A. Maksimenko, D. Desmaële, S. Harrisson, C. Vauthier, P. Couvreur, J. Nicolas, *Biomacromolecules* **2013**, *14*, 2837-2847.

- [17] D. Vinciguerra, A. Degrassi, L. Mancini, S. Mura, J. Mougin, P. Couvreur, J. Nicolas, *Biomacromolecules* **2019**, *20*, 2464-2476.
- [18] S. Zhuo, F. Zhang, J. Yu, X. Zhang, G. Yang, X. Liu, *Molecules* **2020**, *25*, 5649.
- [19] Y. Tao, S. Liu, Y. Zhang, Z. Chi, J. Xu, *Polym. Chem.* **2018**, *9*, 878-884.
- [20] L. Fu, C. Sun, L. Yan, *ACS Appl. Mater. Interfaces* **2015**, *7*, 2104-2115.
- [21] T. Jiang, Y.-M. Li, Y. Lv, Y.-J. Cheng, F. He, R.-X. Zhuo, *Colloids Surf. B: Biointerfaces* **2013**, *111*, 542-548.
- [22] H. Ruan, S. Hao, P. Young, H. Zhang, *Horiz. Cancer Res.* **2015**, *56*, 23-40.
- [23] Y. Li, T. Mei, S. Han, T. Han, Y. Sun, H. Zhang, F. An, *Chin. Chem. Lett.* **2020**, *31*, 3027-3040.
- [24] N. Qiu, X. Liu, Y. Zhong, Z. Zhou, Y. Piao, L. Miao, Q. Zhang, J. Tang, L. Huang, Y. Shen, *Adv. Mater.* **2016**, *28*, 10613-10622.
- [25] T. Fukami, T. Yokoi, *Drug Metab. Pharmacok.* **2012**, *27*, 466-477.
- [26] F. Amissah, R. Duverna, B. J. Aguilar, R. A. Poku, G.-E. Kiros, N. S. Lamango, *Am. J. Cancer Res.* **2014**, *4*, 116-134.
- [27] C. J. Martínez Rivas, M. Tarhini, W. Badri, K. Miladi, H. Greige-Gerges, Q. A. Nazari, S. A. Galindo Rodríguez, R. Á. Román, H. Fessi, A. Elaissari, *Int. J. Pharm.* **2017**, *532*, 66-81.
- [28] P. W. J. M. Frederix, I. Patmanidis, S. J. Marrink, *Chem. Soc. Rev.* **2018**, *47*, 3470-3489.
- [29] N. Singh, W. Li, *Int. J. Mol. Sci.* **2019**, *20*, 3774.
- [30] D. Bochicchio, M. Salvalaglio, G. M. Pavan, *Nat. Commun.* **2017**, *8*, 147.
- [31] E. Weyandt, L. Leanza, R. Capelli, G. M. Pavan, G. Vantomme, E. W. Meijer, *Nat. Commun.* **2022**, *13*, 248.
- [32] A. Sarkar, R. Sasmal, C. Empereur-mot, D. Bochicchio, S. V. K. Kompella, K. Sharma, S. Dhiman, B. Sundaram, S. S. Agasti, G. M. Pavan, S. J. George, *J. Am. Chem. Soc.* **2020**, *142*, 7606-7617.
- [33] I. R. Sasselli, Z. Syrgiannis, N. A. Sather, L. C. Palmer, S. I. Stupp, *J. Phys. Chem. B* **2022**, *126*, 650-659.
- [34] M. Rad-Malekshahi, K. M. Visscher, J. P. G. L. M. Rodrigues, R. de Vries, W. E. Hennink, M. Baldus, A. M. J. J. Bonvin, E. Mastrobattista, M. Weingarh, *J. Am. Chem. Soc.* **2015**, *137*, 7775-7784.
- [35] P. Gao, J. Nicolas, T. Ha-Duong, *J. Am. Chem. Soc.* **2021**, *143*, 17412-17423.
- [36] S. Harrisson, J. Nicolas, A. Maksimenko, D. T. Bui, J. Mougin, P. Couvreur, *Angew. Chem. Int. Ed.* **2013**, *52*, 1678-1682.
- [37] Y. Bao, E. Guégain, J. Mougin, J. Nicolas, *Polym. Chem.* **2018**, *9*, 687-698.
- [38] J. Nicolas, *Chem. Mater.* **2016**, *28*, 1591-1606.
- [39] D. Dheer, J. Nicolas, R. Shankar, *Adv. Drug Deliv. Rev.* **2019**, *151-152*, 130-151.
- [40] E. Di Consiglio, K. Darney, F. M. Buratti, L. Turco, S. Vichi, E. Testai, L. S. Lautz, J. L. C. M. Dorne, *Toxicol. Lett.* **2021**, *350*, 162-170.
- [41] Y. Bao, J. Nicolas, *Polym. Chem.* **2017**, *8*, 5174-5184.
- [42] K. Rose, A. Steinbüchel, *Appl. Environ. Microbiol.* **2005**, *71*, 2803-2812.
- [43] W. Chu, P. Tian, N. Ding, Q. Cai, J. Li, X. Zhuo, Z. Tang, J. Gou, T. Yin, Y. Zhang, H. He, X. Tang, *Pharm. Res.* **2018**, *35*, 230.
- [44] W. M. S. Russell, *Altern. Lab. Anim.* **2000**, *28*, 915-922.